NASA Technical Memorandum 106030

An Experimental Investigation of S-Duct Flow Control Using Arrays of Low Profile Vortex Generators

Bruce A. Reichert and Bruce J. Wendt
Lewis Research Center
Cleveland, Ohio

Prepared for the
31st Aerospace Sciences Meeting and Exhibit
sponsored by the American Institute of Aeronautics and Astronautics
Reno, Nevada, January 11-14, 1993

An Experimental Investigation of S-Duct Flow Control Using Arrays of Low-Profile Vortex Generators

B. A. Reichert* and B. J. Wendt†
NASA Lewis Research Center, Cleveland, Ohio

Abstract

An experimental investigation was undertaken to measure the effect of various configurations of low-profile vortex generator arrays on the flow in a diffusing S-duct. Three parameters that characterize the vortex generator array were systematically varied to determine their effect: (1) the vortex generator height, (2) the streamwise location of the vortex generator array, and (3) the vortex generator spacing. Detailed measurements of total pressure at the duct exit, surface static pressure, and surface flow visualization were gathered for each vortex generator configuration. These results are reported here along with total pressure recovery and distortion coefficients determined from the experimental data. Each array of vortex generators tested improved total pressure recovery. The configuration employing the largest vortex generators was the most effective in reducing total pressure distortion but did not produce the greatest total pressure recovery. No configuration of vortex generators completely eliminated the flow separation that naturally occurs in the S-duct, however the extent of the separated flow region was reduced.

Introduction

The use of geometrically complex ducts is common practice in modern aircraft. S-shaped ducts are often used in aircraft propulsion systems to join the inlet at the airframe to the engine face. Examples of aircraft with inlet S-ducts include the Boeing 727, Lockheed Tristar (L-1011), General Dynamics F-16, and McDonnell-Douglas F-18. Ideally, a diffusing S-duct will efficiently decelerate the flow in order to obtain high static pressure and uniform flow at the engine face with minimal total pressure loss. However, airframe weight and space considerations demand as short a duct as possible, resulting in high degrees of centerline curvature and large changes in cross-sectional area. These factors are responsible for the development of strong secondary flow and attendant boundary layer separation, which increase the total pressure nonuniformity (*i.e.*, distortion) and total pressure loss at the duct exit. Large amounts of distortion significantly reduce engine performance and may lead to drastic results, such as engine stall.

Experimentalists have devoted considerable effort exploring highly three-dimensional compressible flow in diffusing S-ducts. The secondary flow and boundary layer development within a diffusing S-duct were revealed in the study of Vakili *et al.*[1] by cross plane measurements of velocity and total pressure at several axial locations within the duct. A study conducted at NASA Lewis Research Center was reported by Wellborn *et al.*[2] on a geometrically similar, but larger, duct. Both studies have shown that the dominant flow features are a large region of separated flow near the end of the first bend and a pair of counter-rotating axial vortices at the duct exit. The relationship between these two flow features and their relative contribution to distortion and total pressure loss are unclear.

The concept of using vortex generators to reduce or eliminate boundary layer separation has been known for many years. Early studies of vortex generators have focused on improving diffuser performance. Substantial improvements in pressure recovery were reported by Taylor[3] and Brown[4] on various subsonic diffuser geometries. Work done at NASA Lewis Research Center on a mixed-compression inlet by Mitchell and Davis[5] established the principle of using vortex generator arrays as a means of reducing exit airflow distortion. Studying the same diffusing S-duct used in their previous study, Vakili *et al.*[6] showed that an array of vane type vortex generators reduced total pressure distortion at the duct exit.

Recent work on the design and performance of vortex generators has produced "low-profile" vortex generators that match or exceed the mixing performance of the more conventional vane type generators.[7] In the present study various configurations of low-profile vortex generator arrays were installed in the NASA Lewis Research Center diffusing S-duct. Three parameters that characterize the vortex generator array were systematically varied: (1) the vortex generator height, (2) the streamwise location of the vortex generator array, and (3) the vortex generator spacing. Detailed measurements of total pressure at the duct exit, surface static pressure, and surface flow visualization were gathered for each vortex generator configuration. The objectives of this study are to determine the effect of the variation of the vortex generator array parameters on the flow in a diffusing S-duct and to gain additional insight into the relationship between flow separation, axial vortices, distortion and total pressure loss.

---

*Aerospace Engineer, Inlet, Duct, and Nozzle Flow Physics Branch.

†Aerospace Engineer, National Research Council Associate, Member AIAA.

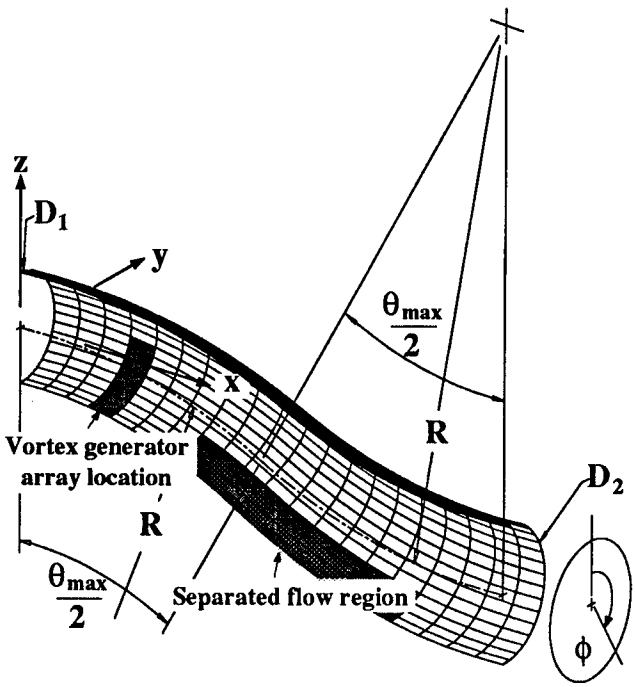

Fig. 1 Geometry of the diffusing S-duct

Experimental Facilities and Techniques

Diffusing S-Duct

The geometry of the diffusing S-duct examined in this study is shown in Fig. 1. The duct centerline is defined by two circular arcs with an identical radius of curvature, $R = 102.1$ cms and subtended angle $\theta_{max}/2 = 30°$. Both arcs lie within the xz-plane as shown in Fig. 1. The coordinates (x_{cl}, y_{cl}, z_{cl}) of the duct centerline are given by Eqs. (1, for $0 \leq \theta \leq \theta_{max}/2$) and (2, for $\theta_{max}/2 \leq \theta \leq \theta_{max}$) :

$$\begin{aligned} x_{cl} &= R\sin\theta \\ y_{cl} &= 0 \\ z_{cl} &= R\cos\theta - R \end{aligned} \tag{1}$$

$$\begin{aligned} x_{cl} &= 2R\sin\left(\frac{\theta_{max}}{2}\right) - R\sin\left(\theta_{max} - \theta\right) \\ y_{cl} &= 0 \\ z_{cl} &= 2R\cos\left(\frac{\theta_{max}}{2}\right) - R - R\cos\left(\theta_{max} - \theta\right) \end{aligned} \tag{2}$$

The cross-sectional shape of the duct perpendicular to the centerline is circular. The diameter of the cross section varies with the arc angle θ and is given by Eq. (3):

$$\begin{aligned} \frac{D}{D_1} = 1 &+ 3\left(\frac{D_2}{D_1} - 1\right)\left(\frac{\theta}{\theta_{max}}\right)^2 \\ &- 2\left(\frac{D_2}{D_1} - 1\right)\left(\frac{\theta}{\theta_{max}}\right)^3 \end{aligned} \tag{3}$$

In Eq. (3) and Fig. 1 $D_1 = 20.4$ cms is the radius at the duct inlet and $D_2 = 25.1$ cms is the radius at the duct exit. This provides an exit to inlet area ratio of $A_2/A_1 = 1.52$. The offset of the duct resulting from the centerline curvature is $1.34D_1$, and the length of the duct measured along the centerline is $5.23D_1$.

When discussing experimental results, axial location will refer to distance to cross stream planes measured along the duct centerline and normalized by the duct inlet diameter, s/D_1. Position within cross stream planes is specified by the polar angle ϕ, measured from the vertical in a positive clockwise direction as shown in Fig. 1, and the radial distance from the centerline r.

Vortex Generator Array

The study of vane type vortex generators by Wendt *et al.*[8] indicated that the mixing performance of a vortex generator array is determined by the strength and downstream interaction of the resultant vortices. The strength of the resultant vortices is determined mostly by the generator size. The downstream interaction between resultant vortices is determined by the spacing between generators in an array. Tight arrays of embedded vortices provide the best local mixing but are quickly attenuated as the flow proceeds downstream.

The low-profile vortex generators used in this study are wishbone type generators. A flow visualization study by Lin *et al.*[7] indicates that each generator forms a pair of counter-rotating vortices with the flow between vortices directed upwards, away from the wall (a common upflow pair). Fig. 2 illustrates the geometry of these devices and the geometric parameters of the arrays. All of the vortex generators tested were geometrically similar (*i.e.* the ratios λ/c and h/c are constant). Three parameters define the vortex generator array: (1) the generator size, which is characterized by the generator height, h/D_1, (2) the axial placement of the vortex generator array in the duct, s/D_1, and (3) the relative spacing between the vortex generators, l/λ. Single cross stream arrays of these vortex generators were tested. In this study each parameter was varied while the other two were held

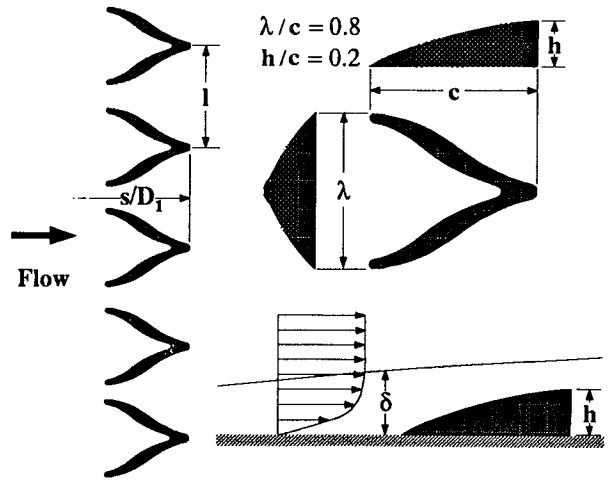

Fig. 2 Vortex generator array geometry

constant in order to ascertain the separate effect of each parameter. The test configurations are summarized in Table 1. Note that the middle configuration for each parameter variation is identical. A representative location of the vortex generator arrays in the S-duct is shown in Fig. 1. The axial placement of the vortex generator arrays was near the region of separation that occurs in the duct without vortex generators installed ($2.02 \leq s/D_1 \leq 4.13$ at $\phi = 180°$), as is indicated in Fig. 1.

The vortex generator arrays span the angular range $80° \leq \phi \leq 280°$. For the repeated middle configuration ($s/D_1 = 1.6$, $h/D_1 = 3.89$, $l/\lambda = 2.56$), eight vortex generators were used. The criterion used to determine the circumferential or angular span of the vortex generator array was developed by studying the surface flow visualization for flow without vortex generators, Fig. 3, and in particular the streamlines that terminate in the reattachment node, shown in Fig. 3 as dashed lines. At an axial location of $s/D_1 = 1.6$ these streamlines lie at approximately $\phi = 80°$ and $\phi = 280°$. Flow within these two streamlines, at least very near the duct surface, becomes captured in the spiral node and separates from the duct surface. The criterion was determined prior to the vortex generator testing. The validity of the criterion is discussed in the Results and Discussion section. All vortex generator configurations employed an even number of vortex generators, so that no vortex generator was located at $\phi = 180°$. This was done because the vortex generators produce a common upflow pair of vortices which we believed would reinforce rather than mitigate the pair of naturally occurring counter-rotating vortices, whereas vortex generators placed symmetrically on either side of $\phi = 180°$ would result in downflow along $\phi = 180°$.

Facility Flow Conditions

Experimental measurements of the duct flow field are made at NASA Lewis Research Center using the

	h/D_1	s/D_1	l/λ
Height	1.55%	1.6	2.56
	3.89%	1.6	2.56
	6.22%	1.6	2.56
Location	3.89%	1.1	2.56
	3.89%	1.6	2.56
	3.89%	2.1	2.56
Spacing	3.89%	1.6	1.43
	3.89%	1.6	2.56
	3.89%	1.6	3.70

Table 1 Summary of vortex generator array parameters tested

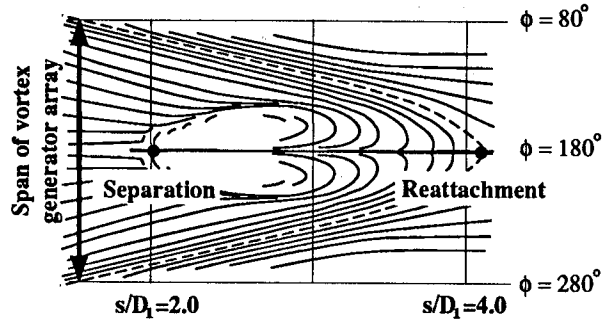

Fig. 3 Surface flow visualization without vortex generators

Internal Fluid Mechanics Facility. This facility is designed to support the research of a variety of internal flow configurations and is described in detail by Porro *et al.*[9] Smooth circular pipes of appropriate diameter are attached upstream and downstream of the S-duct to provide a uniform incoming flow and a smooth, continuous condition for flow exiting the duct. The lengths of the upstream and downstream pipes are each $3.75D_1$. The duct inlet Mach number is $M = 0.6$ for all experimental test conditions and measurements. The inlet boundary layer thickness is approximately 4% of the duct inlet diameter and the Reynolds number, based on inlet diameter, is approximately $Re_{D_1} = 2.6 \times 10^6$.

Measurement Techniques

Surface static pressures inside the S-duct were recorded by a grid of 220 taps located on axial lines at angles $\phi = 10°$, $90°$, and $170°$, as well as circumferential lines at $s/D_1 = 0.96$, 2.97, and 4.01. Total pressure in the cross stream plane at the duct exit was recorded by a Pitot probe rake traversed radially and circumferentially to acquire 720 measurements on a uniform (r, ϕ) grid. Grid resolution on the radial axis was $\Delta r/D_2 = 0.025$ and $\Delta\phi = 10°$ circumferentially. Visualization of duct near-surface flows was achieved by a fluorescent oil dot technique. The flow pattern revealed by the oil dots was photographed and then digitized with an image scanner to produce the results shown here.

Results and Discussion

Static and total pressure plots are presented as pressure coefficients defined by Eqs. 4 and 5. The pressures p_0 and p represent the local values of total and static pressure. The reference variables, subscripted *ref*, were evaluated on the duct centerline at a location one-half duct diameter upstream of the S-duct inlet ($s/D_1 = -0.5$).

$$C_p = \frac{p - p_{ref}}{p_{0,ref} - p_{ref}} \tag{4}$$

$$C_{p_0} = \frac{p_0 - p_{ref}}{p_{0,ref} - p_{ref}} \tag{5}$$

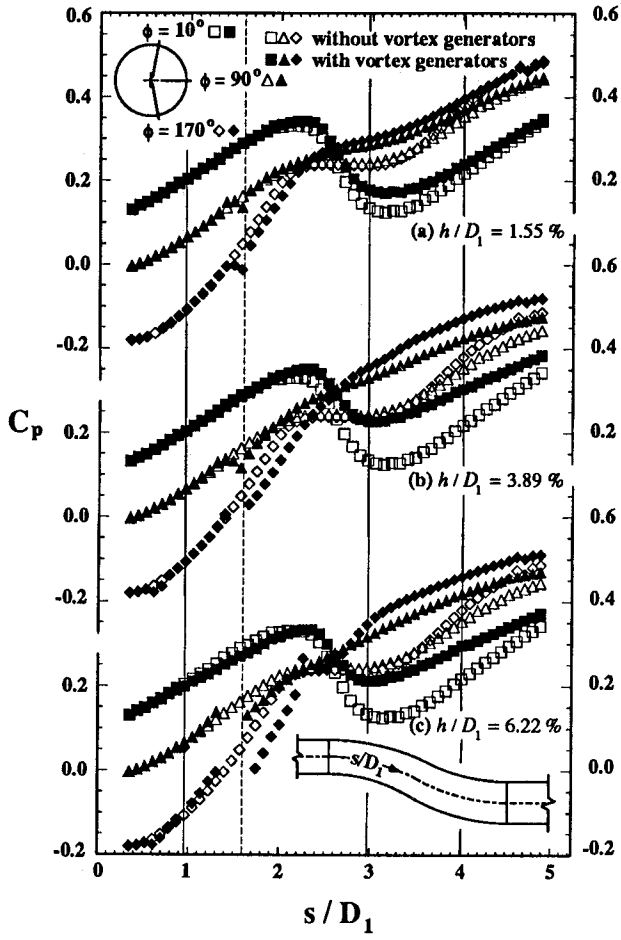

Fig. 4 Axial static pressure coefficient for variation of vortex generator height

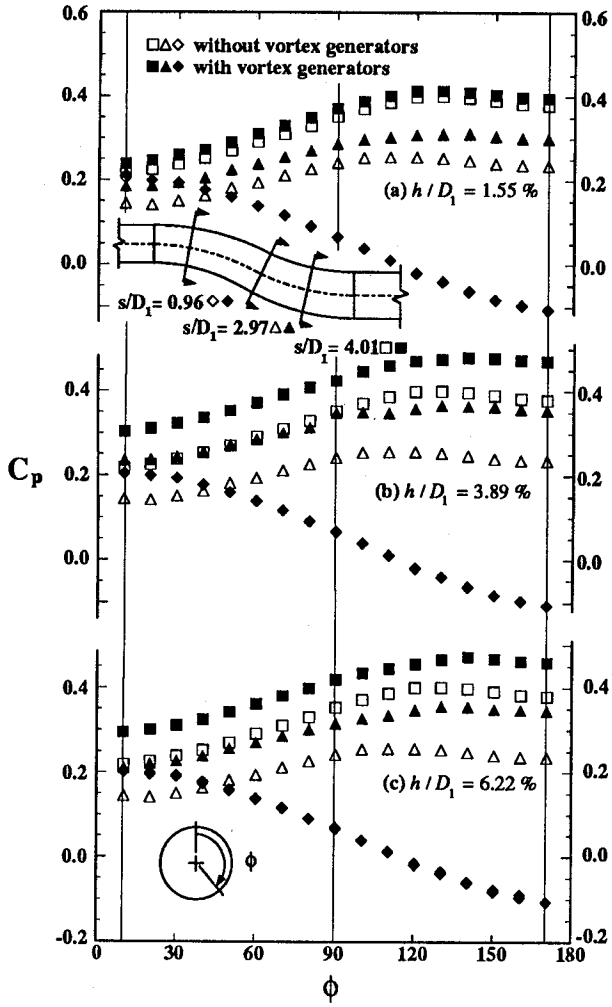

Fig. 5 Circumferential static pressure coefficient for variation of vortex generator height

Near the duct exit (at $s/D_1 = 5.73$), an area averaged total pressure recovery factor, $p_0/p_{0,ref}$, was determined by integrating the total pressure data over the entire duct cross stream plane. A similar total pressure average was also determined by Eq. 6, where the integration is only over a pie-shaped segment of the cross stream plane of angular extent ϕ. The segment that results in the lowest value of $\overline{p_0}(\phi)/p_{0,ref}$ is used in Eq. 7 to determine the distortion coefficient $DC(\phi)$. The denominator of Eq. 7 is the dynamic pressure averaged over the entire duct cross stream plane. The values of ϕ used in this study are 60°, 90°, and 120°.

$$\overline{p_0}(\phi)/p_{0,ref} = \frac{\int_{\phi} (p_0/p_{0,ref})dA}{\int_{\phi} dA} \qquad (6)$$

$$DC(\phi) = \frac{\overline{p_0} - \overline{p_0}(\phi)}{\overline{q}} \qquad (7)$$

Vortex Generator Height

Figs. 4 and 5 show values of axial and circumferential static pressure for three different values of the vortex generator height parameter h/D_1. The axial location and spacing parameters s/D_1 and l/λ remained constant for the three results presented. In addition to the three heights reported here an array of smaller vortex generators with a height of $h/D_1 = 0.62\%$ was also tested. The results for this configuration differed only slightly from flow without vortex generators and are not presented. In Figs. 4 and 5 the vortex generator results (plotted with solid symbols) are compared with static pressure measurements for flow without vortex generators (plotted with open symbols). The dashed vertical line in Fig. 4 indicates the axial location of the vortex generator array. The solid vertical lines in Fig. 4 mark the axial location of the circumferential static pressure taps whose values are shown in Fig. 5. Likewise, in Fig. 5 the solid vertical lines mark the circumferential location of the axial static pressure taps whose results are displayed in Fig. 4.

For flow without vortex generators, the constant values of static pressure in Fig. 4 at $2 < s/D_1 < 3$ for $\phi = 90°$ and 170° are associated with the flow separation. The effect of the separated flow is also evident in Fig. 5 for the circumferential static pressure

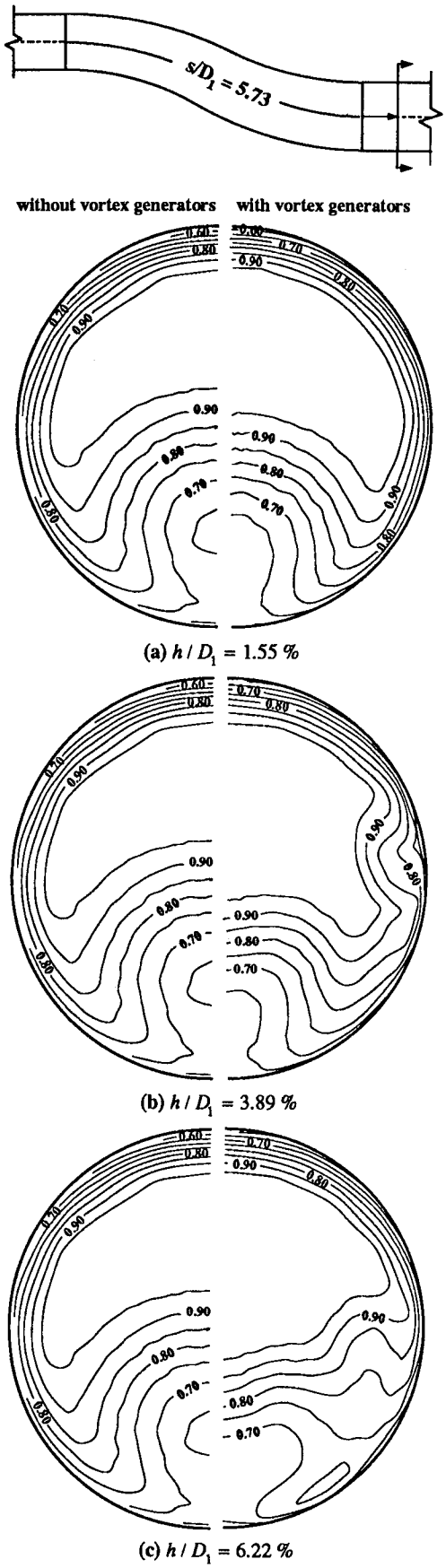

Fig. 6 Total pressure coefficient contours at $s/D_1 = 5.73$ for variation of vortex generator height

at $s/D_1 = 2.97$ and 4.01, which lie within the region of separated flow. Peak values of static pressure were observed at $\phi = 100°$ ($s/D_1 = 2.97$) and $\phi = 120°$ ($s/D_1 = 4.01$). For unseparated flow, the pressure there should increase monotonically for increasing values of ϕ with the maximum static pressure at $\phi = 180°$.

The results in Fig. 4 show significantly higher values of static pressure for flow with vortex generators in the region $2 < s/D_1 < 4$. In Fig. 4(a) the static pressure values nearly return to the levels without vortex generators at $s/D_1 > 4$ whereas in Figs. 4(b) and (c) the static pressure values remain considerably higher than the values for flow without vortex generators. This trend is clear in Fig. 5, particularly in the data at $s/D_1 = 4.01$. This would suggest that the smallest configuration of vortex generators is reducing flow blockage in the separated flow region but not at the exit, whereas the larger generators are, to some extent, also reducing flow blockage at the exit. In Fig. 5(b) and particularly Fig. 5(c) it appears that the circumferential extent of the separation is reduced. In Fig 5(c) the peak values of static pressure appear at $\phi = 130°$ and $\phi = 140°$ for $s/D_1 = 2.97$ and 4.01 (*c.f.* $\phi = 100°$ and $\phi = 120°$ for flow without vortex generators). In Figs. 4(a) and (b) there is no perceptible upstream influence of static pressure caused by the vortex generator arrays. In Fig. 4(c) the flow appears to be accelerating upstream of the vortex generator array as a result of their blockage.

Contours of total pressure near the duct exit (at $s/D_1 = 5.73$) are shown in Fig. 6. In each case the duct cross section is split vertically to show total pressure contours for flow without vortex generators on the left side and for flow with vortex generators on the right side. The large region of diminished total pressure in the lower duct half results from the pair of naturally occurring counter-rotating vortices convecting low momentum fluid away from the duct walls. Fig. 6(a) shows that the smallest vortex generators have only slightly reduced the region of diminished total pressure. The shape of the region remains the same but the total pressure contour levels appear approximately 0.05 higher for flow with vortex generators. For the larger generators, Fig. 6(b) and (c), the region of diminished total pressure (hence flow blockage) is significantly reduced by the vortex generators. Also, the effect of the vortex generators on the boundary layer can be seen at the 3 o'clock position of Fig. 6(b).

Surface flow visualization results are shown in Fig. 7. The region shown in Fig. 7 approximately corresponds to the area labeled "separated flow region" on Fig. 1. The flow in Fig. 7 is from left to right. There is little discernible difference in the pattern observed between flow with the smallest vortex generator, Fig. 7(a), and flow without vortex generators, Fig. 3. The familiar spiral node associated with three-dimensional separation is readily apparent. As the vortex generator height is

Configuration	$\overline{p_0}/p_{0,ref}$	$DC(60)$	$DC(90)$	$DC(120)$
No vortex generators	96.71%	41.55%	35.72%	28.91%
$h/D_1 = 1.55\%$	96.89%	49.07%	41.37%	32.03%
$h/D_1 = 3.89\%$	97.07%	46.04%	38.25%	29.58%
$h/D_1 = 6.22\%$	96.80%	37.78%	35.06%	31.35%

Table 2 Total pressure recovery and distortion for variation of vortex generator height

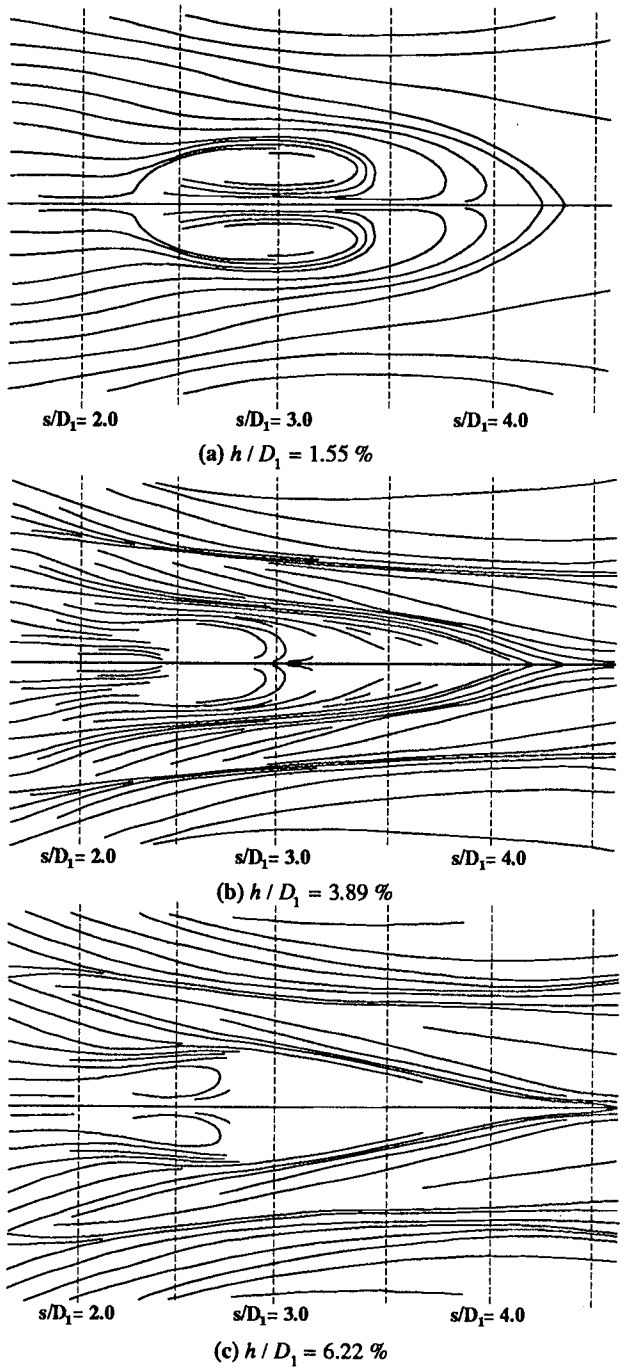

Fig. 7 Surface flow visualization for variation of vortex generator height

increased, Fig. 7(b) and (c), several phenomena are observed. First, the location of the beginning of separation appears to move further downstream. Second, the angular extent of the separation appears to diminish. Finally, the magnitude of the cross flow near the separation is reduced. The effect of the vortices produced by the vortex generators may be seen in the nearly straight trailing lines. Although the size of the separation is reduced with increasing vortex generator height, separation still exists to some extent for all three cases.

Table 2 is a summary of the performance coefficients calculated from the total pressure data presented in Fig. 6 for flow without vortex generators and for the three different vortex generator heights. Total pressure recovery is improved by each vortex generator array configuration. The greatest total pressure recovery improvement did not result from the array with the largest vortex generators, but rather from the mid-sized configuration. The mid-sized vortex generator height is approximately equal to the boundary layer thickness at their installed location. Whereas total pressure recovery was improved by all vortex generator arrays, the distortion, as measured by the $DC(60)$, $DC(90)$, and $DC(120)$ parameters, was adversely affected by the smallest two configurations of vortex generator arrays. However, the distortion parameters are generally improving for increasing vortex generator height which suggests that further distortion improvement could be obtained by still larger vortex generators.

Vortex Generator Axial Location

For the results presented in this section, only the axial location of the vortex generator array was varied while their height and spacing remained fixed. Here the trends and their significance are a little more obvious. As the axial location of the vortex generator array approaches the separation point for flow without vortex generators ($s/D_1 = 2.02$) the effect of the vortex generator array diminished rapidly. This is particularly noticeable in the static pressure plots, Figs. 8 and 9. Dashed vertical lines in Fig. 8 indicate the location of the vortex generator array. Little difference exists between the flows with vortex generator axial locations at $s/D_1 = 1.1$ and $s/D_1 = 1.6$. Both locations produce a flow with static pressure markedly higher than exists in the flow without vortex generators, particularly in the separated flow region. For the array of vortex generators at $s/D_1 = 2.1$ however, the static pressure is nearly as low as that for

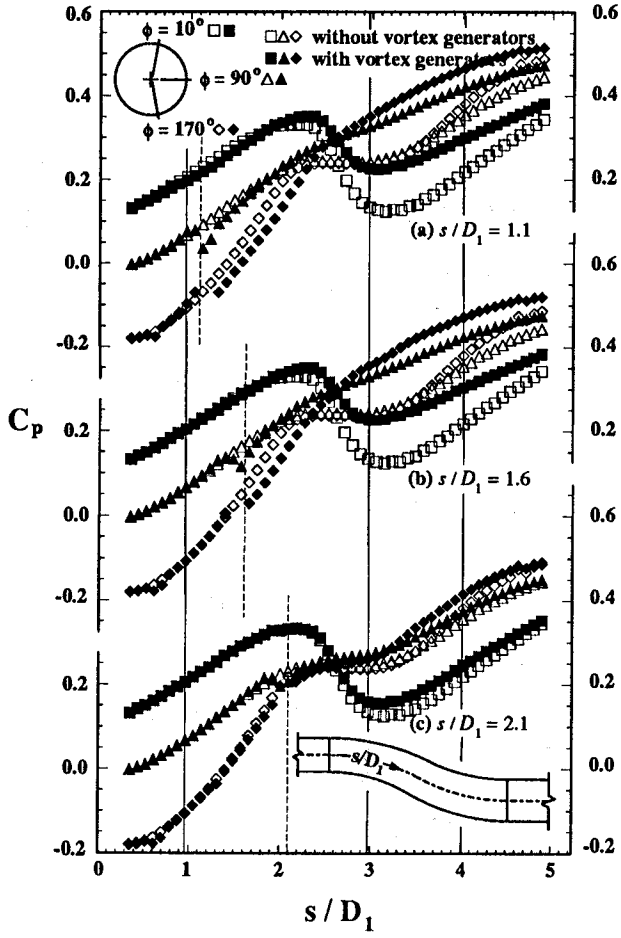

Fig. 8 Axial static pressure for variation of axial location of vortex generator

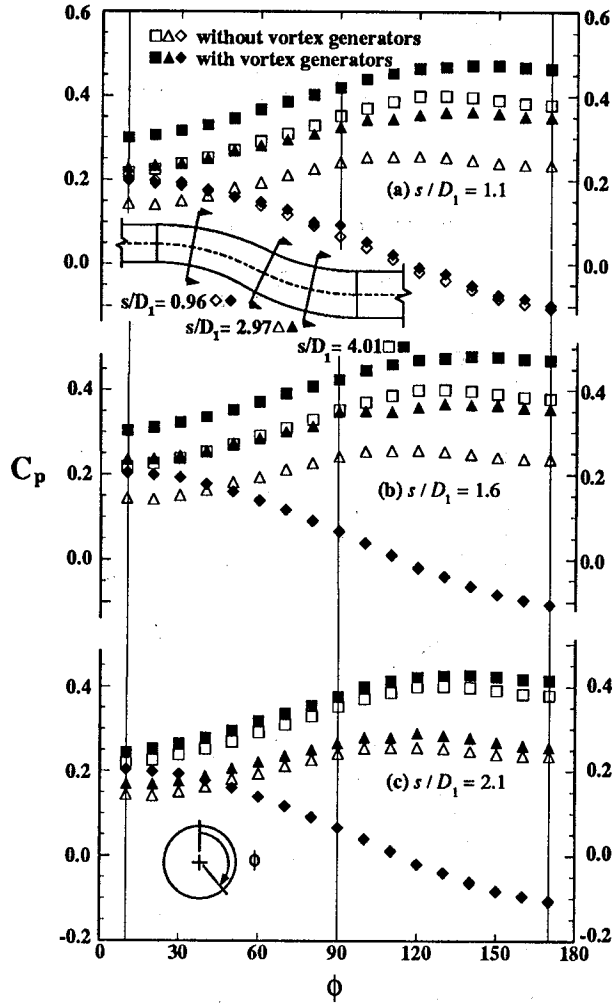

Fig. 9 Circumferential static pressure coefficient for variation of axial location of vortex generator

flow without vortex generators. Based on static pressure data this configuration of vortex generators was the least effective of all configurations tested in this study. It may be that the array of vortices requires some interaction distance along the streamwise direction to affect the flow field in the vicinity of separation. Another reason for the poor performance at $s/D_1 = 2.1$ may concern the strength of the generated vortices. Low velocity fluid this close to the separated region may not produce vortices of sufficient strength to provide the needed mixing and secondary flow interaction responsible for the improved performance exhibited by arrays mounted further upstream in the duct. The location of the peak values of static pressure in Fig. 9 indicates that the arrays at $s/D_1 = 1.1$ and $s/D_1 = 1.6$ are reducing the circumferential span of the separated region at $s/D_1 = 2.97$ and $s/D_1 = 4.01$.

Total pressure contours shown in Fig. 10 for vortex generator arrays installed at $s/D_1 = 1.1$ and $s/D_1 = 1.6$ appear very similar. Compared to flow without vortex generators, the distance that the region of diminished total pressure extends away from the wall in the lower duct half has been greatly reduced. This is not the case for $s/D_1 = 2.1$, where the region of diminished total pressure is comparable to flow without vortex generators. In all three cases, the effect of the outer most vortex generator in the array can be seen in the total pressure contours at approximately the 3 o'clock position. From the results in Fig. 10 it appears that the outer most vortex generators that are responsible for this disturbance may be unnecessary and are adversely affecting the flow.

The surface flow visualization shown in Fig. 11 indicates that for arrays of vortex generators located at $s/D_1 = 1.6$ the region of separated flow becomes narrower and the separation point moves downstream. These trends are also observed for the array located at $s/D_1 = 1.1$ although the results are not as pronounced. The results for the array located at $s/D_1 = 2.1$ differ very little from visualization of the flow without vortex generators (Fig. 3). None of the configurations was successful in eliminating flow separation.

The performance characteristic for variation in vortex generator axial location are summarized in Table 3. All three cases result in higher total pressure recovery and higher static pressure, with cases $s/D_1 = 1.1$ and $s/D_1 = 1.6$ producing significant improvement. None

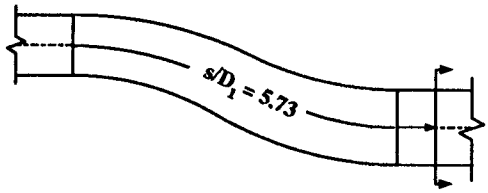

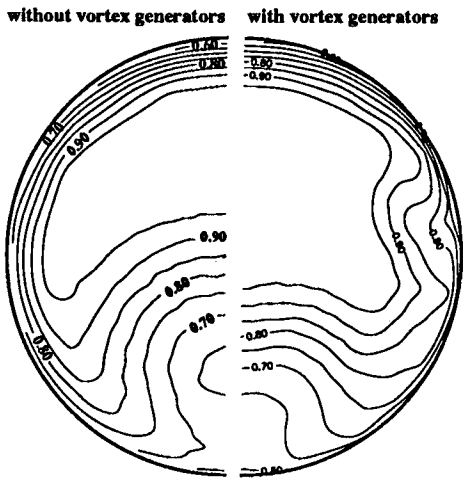

(a) $s / D_1 = 1.1$

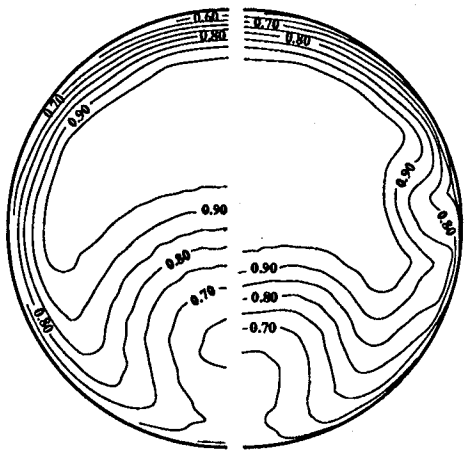

(b) $s / D_1 = 1.6$

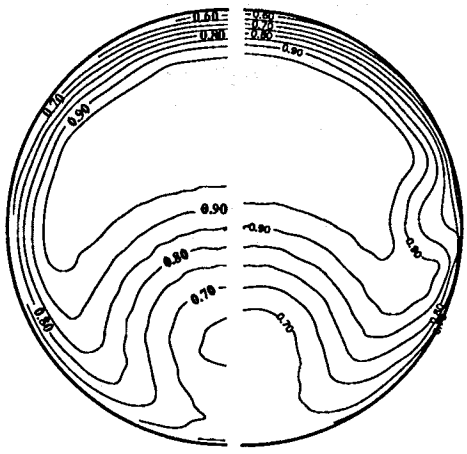

(c) $s / D_1 = 2.1$

Fig. 10 Total pressure coefficient contours at $s/D_1 = 5.73$ for variation of axial location of vortex generator

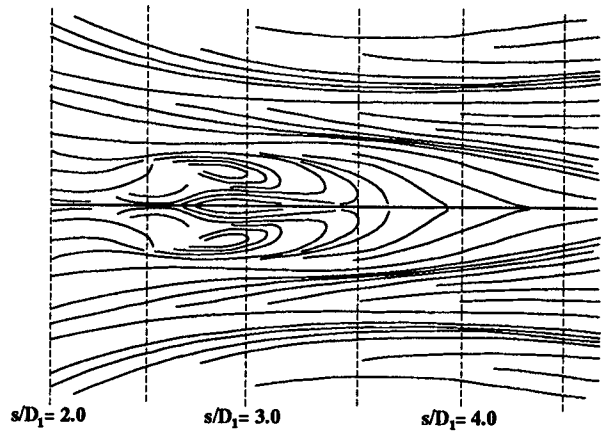

(a) $s / D_1 = 1.1$

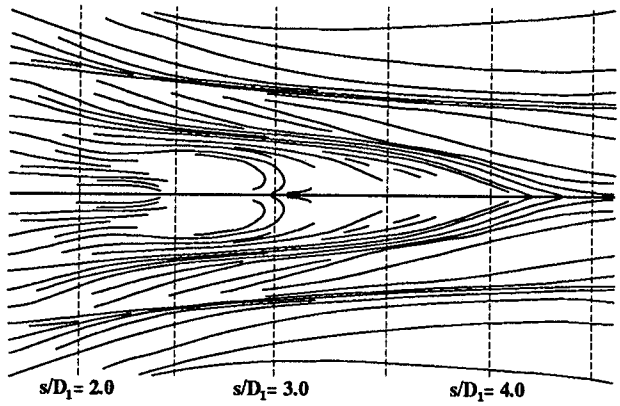

(b) $s / D_1 = 1.6$

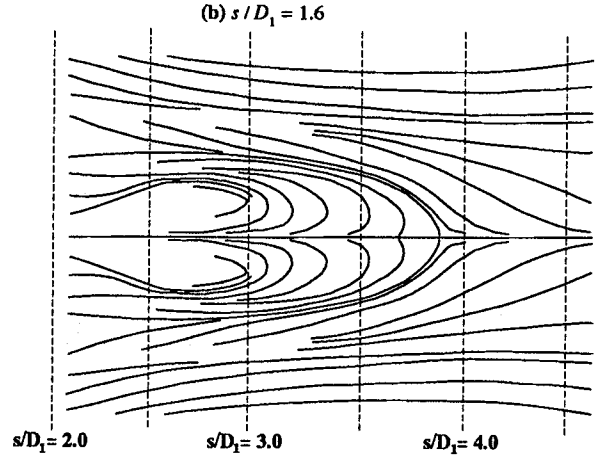

(c) $s / D_1 = 2.1$

Fig. 11 Surface flow visualization for variation of axial location of vortex generator

of the three axial locations lowered distortion below the level without vortex generators as measured by the distortion descriptors given in Table 3. The results suggest that little further improvement in vortex generator array effectiveness can be obtained by studying additional axial locations. As a guideline, it appears that if the location of separation is not precisely known, there is only a small penalty for locating the vortex generators moderately further upstream of the separation than is ideally required.

Configuration	$\overline{p_0}/p_{0,ref}$	$DC(60)$	$DC(90)$	$DC(120)$
No vortex generators	96.71%	41.55%	35.72%	28.91%
$s/D_1 = 1.1$	96.97%	44.72%	37.74%	29.11%
$s/D_1 = 1.6$	97.07%	46.04%	38.25%	29.58%
$s/D_1 = 2.1$	96.75%	43.08%	37.26%	30.05%

Table 3 Total pressure recovery and distortion for variation of axial location of vortex generator

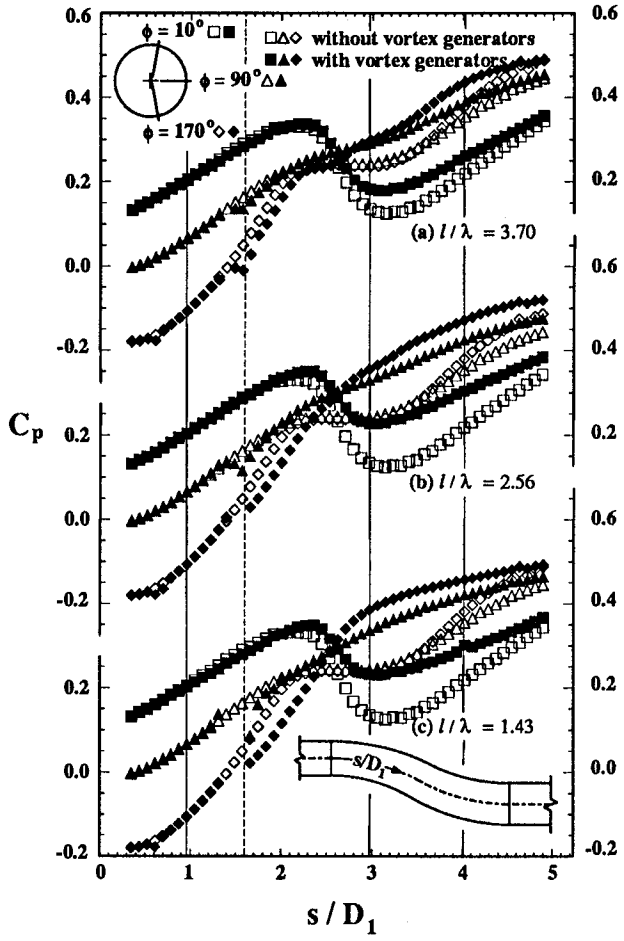

Fig. 12 Axial static pressure for variation of vortex generator spacing

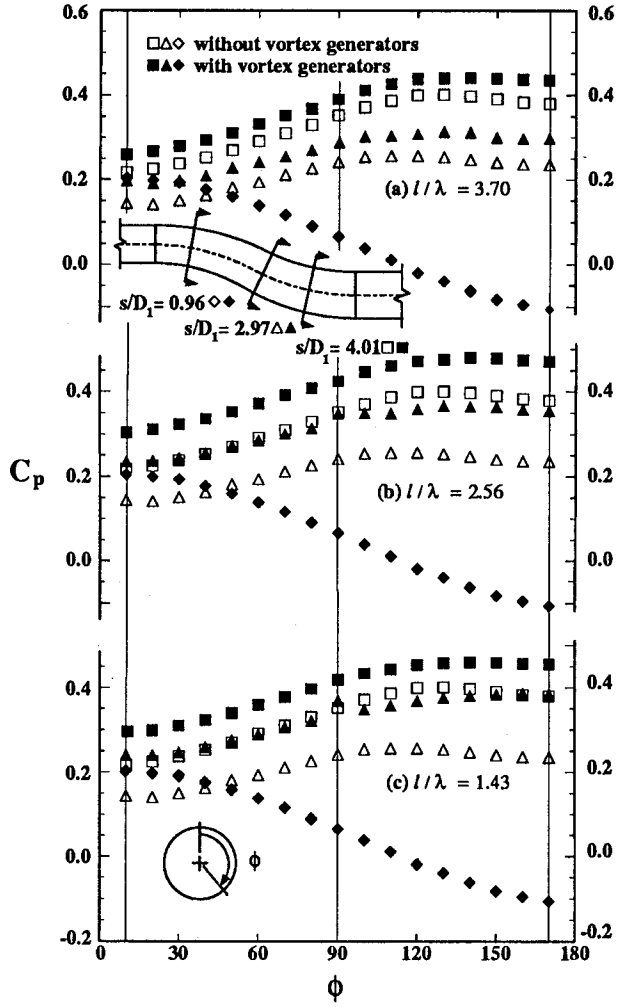

Fig. 13 Circumferential static pressure for variation of vortex generator spacing

Vortex Generator Spacing

For the results presented in this section, only the spacing between vortex generators within the array was varied while their height and axial location remained fixed. The configuration with the closest spacing of vortex generators, $l/\lambda = 1.43$, appeared to be the most effective in reducing separation. This can be seen by examining Fig. 12(c) and comparing the difference in static pressure at $\phi = 170°$ near $s/D_1 = 3$ for flow with and without vortex generators. This is the largest increase of static pressure at this location for any configuration tested. Also, Fig. 13(c) shows the circumferential static pressure at $s/D_1 = 2.97$ achieves it maximum value at $\phi = 170°$ which is for all configurations the largest angle at which the peak static pressure occurs, indicating the greatest reduction in the circumferential extent of separation. Unfortunately, the dramatic increase of static pressure does not extend to the duct exit, where the static pressure at $\phi = 170°$ is nearly equal to the value without vortex generators. This may be partly due to the blockage created by the large number of vortex generators used for this configuration and the associated total pressure loss. For the most widely spaced vortex generator array ($l/\lambda = 3.70$) the static pressure results in Figs. 12(a) and 13(a) indicate lower static pressure, both in the separated flow region and at the duct exit, when compared to the

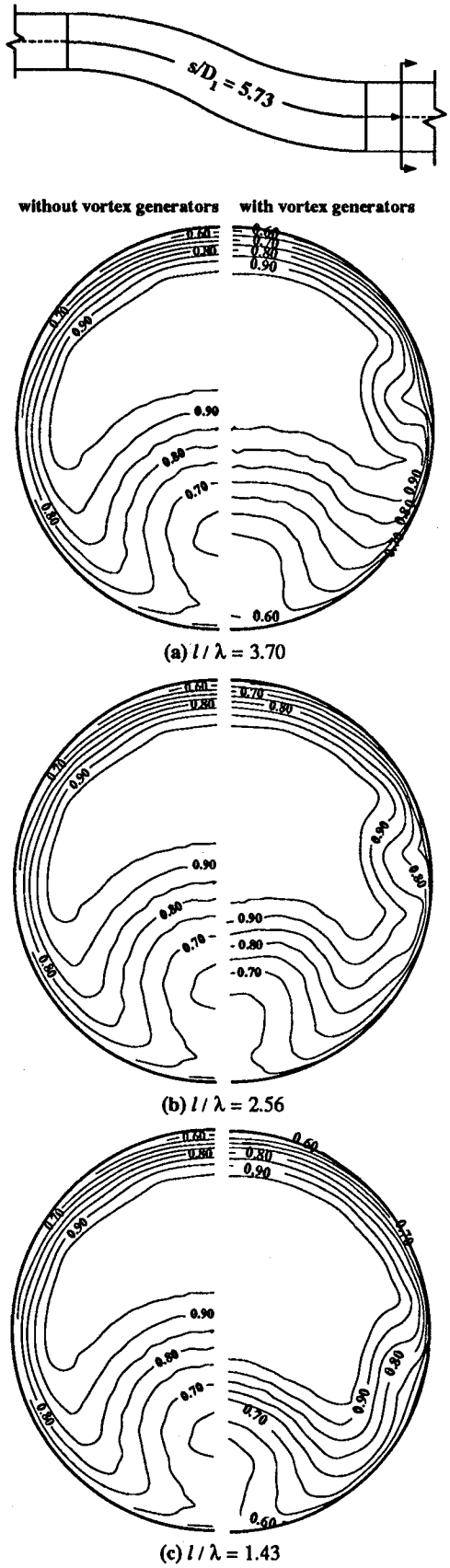

Fig. 14 Total pressure coefficient contours at $s/D_1 = 5.73$ for variation of vortex generator spacing

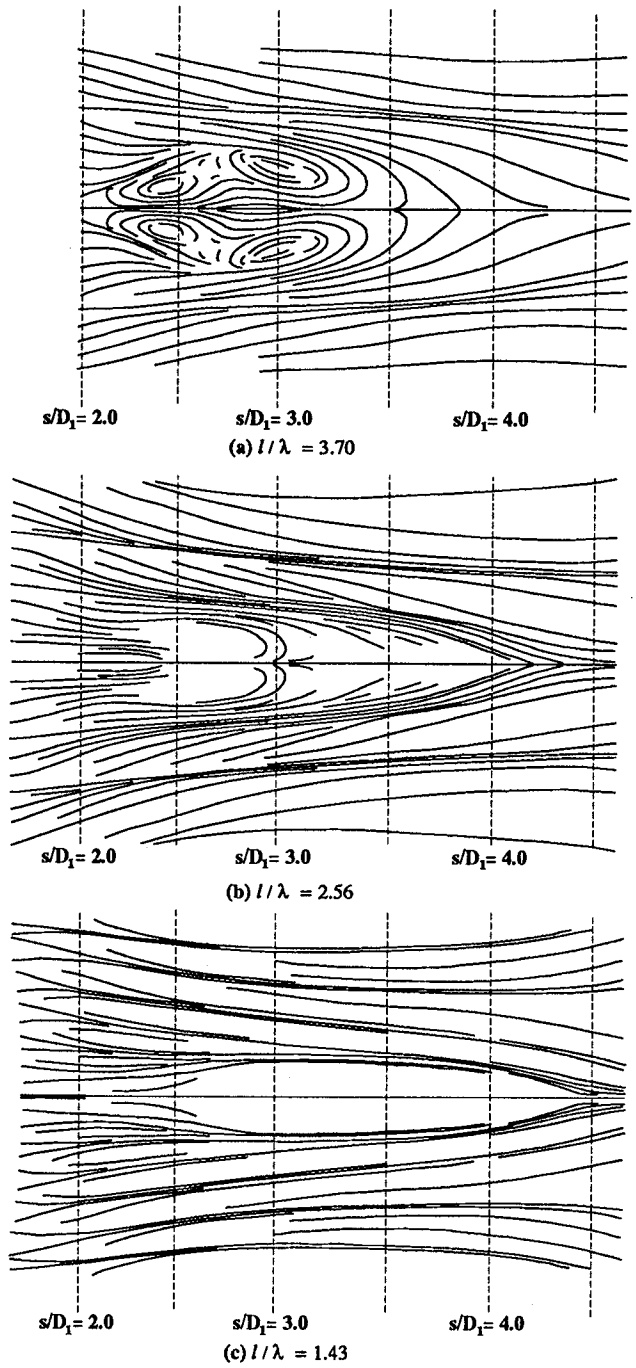

Fig. 15 Surface flow visualization for variation of vortex generator spacing

medium spaced array ($l/\lambda = 2.56$). On average, the highest static pressure at the duct exit results from the medium spaced configuration, Fig 12(b).

The total pressure contours shown in Fig. 14 show that as the vortex generator spacing is decreased, the cross-sectional area where the total pressure coefficient is greater than 0.95 increases, suggesting improved total pressure recovery. However, for the array with the widest and narrowest vortex generator spacing, Figs. 14(a) and (c), the area where the total pressure coefficient is less than 0.65 has also increased when compared to the

Configuration	$\overline{p_0}/p_{0,ref}$	$DC(60)$	$DC(90)$	$DC(120)$
No vortex generators	96.71%	41.55%	35.72%	28.91%
$l/\lambda = 3.70$	96.76%	48.66%	41.82%	33.27%
$l/\lambda = 2.56$	97.07%	46.04%	38.25%	29.58%
$l/\lambda = 1.43$	96.88%	48.27%	38.57%	28.93%

Table 4 Total pressure recovery and distortion for variation of vortex generator spacing

medium spaced configuration, Fig. 14(b). Also, the gradients in total pressure increase as the vortex generator spacing is reduced and are strongest in Fig. 14(c) in comparison to all configurations tested. Again, it appears that the outer most vortex generators of the array are unnecessary and are perhaps detrimental to the flow.

The surface flow visualization shown in Fig. 15 appears to confirm the observation that the configuration with the closest spacing of vortex generators has the greatest effect on reducing separation. Although the widely spaced vortex generator test case does not reduce the size of the separated region it significantly changes its structure. In all cases the separation appears to be contained circumferentially within the trailing streamline that lies behind the pair of vortex generators that lie on either side of the duct half. The flow visualization patterns again emphasize the intricate interaction between the vortices generated by the vortex generators and the secondary flow structures in the region of separation.

The performance characteristic for variation of vortex generator spacing are summarized in Table 4. Total pressure recovery was improved by each configuration of vortex generators. It appears that in general the $DC(120)$ distortion coefficient may continue to improve as the vortex generator spacing is reduced.

Conclusions

As the vortex generator height is increased, the circumferential extent of the separated flow region is reduced (as evidence by circumferential static pressure and surface flow visualization). However, the greatest improvement in total pressure recovery resulted from the mid-sized configuration with vortex generators whose heights are approximately equal to the boundary layer height at their installed location. On the other hand, distortion continued to improve when the vortex generator height was increased.

As the axial location of the vortex generator array nears the location of flow separation, the effectiveness of the vortex generators is greatly reduced. As a guideline, it appears that if the location of separation is not precisely known, there is only a small penalty for locating the vortex generators moderately further upstream of the separation than is ideally required.

As the spacing between vortex generators within the array is reduced the circumferential extent of the separated flow region is reduced. However, the vortex generator array that appeared most effective in reducing separation did not produce the best performance as measured by total pressure recovery or the distortion coefficients.

Although the circumferential span of the vortex generator array was not a parameter that was varied, the total pressure contours indicate that total pressure recovery and distortion may improve if the circumferential span of the array was reduced from the range of $80° \leq \phi \leq 280°$ used in this study.

No vortex generator array configuration tested was successful in completely eliminating flow separation. However, in most cases the circumferential extent of the separation was reduced and in all cases the separation appeared to lie within the trailing streamline behind the pair of vortex generators that lie on either side of the duct half. This suggests that perhaps further reduction of the separation could be affected by placing these two vortex generators even closer.

Acknowledgments

We are grateful for the assistance provided by R. Davis, R. Gronski, W. Hingst, K. Kesey, A. Porro, S. Wellborn, and K. Zaman.

References

[1] Vakili, A. D., Wu, J. M., Liver, P., and Bhat, M. K., "Experimental Investigation of Secondary Flows in a Diffusing S-Duct," The University of Tennessee Space Institute Tech. Rep. UTSI 86/14, 1984.

[2] Wellborn, S. R., Reichert, B. A., and Okiishi, T. H., "Aerodynamic Measurement of the Subsonic Flow Through a Diffusing S-Duct," AIAA Paper 92-3622, 1992. (Also NASA TM 105809).

[3] Taylor, H. D., "Retractable Vortex Generators," United Aircraft Corporation Research Department Report M-15355-3, 1950.

[4] Brown, A. C., "Subsonic Diffusers Designed Integrally with Vortex Generators," *Journal of Aircraft*, Vol. 5, 1968, pp. 221–229.

[5]Mitchell, G. A. and Davis, R. W., "Performance of Centerbody Vortex Generators in an Axisymmetric Mixed Compression Inlet at Mach Numbers From 2.0 to 3.0," NASA TN D-4675, 1968.

[6]Vakili, A. D., Wu, J. M., Liver, P., and Bhat, M. K., "Experimental Investigation of Secondary Flows in a Diffusing S-Duct with Vortex Generators," The University of Tennessee Space Institute Preliminary Copy Final Report for NASA Contract NAG3 233, July 1986.

[7]Lin, J. C., Howard, F. G., and Selby, G. V., "Turbulent Flow Seperation Control Through Passive Techniques," AIAA Paper 89-0976, 1990.

[8]Wendt, B. J., Greber, I., and Hingst, W. R., "The Structure and Development of Streamwise Vortex Arrays Embedded in a Turbulent Boundary Layer," AIAA Paper 92-0551, 1992.

[9]Porro, A. R., Hingst, W. R., Wasserbauer, C. A., and Andrews, T. B., "The NASA Lewis Research Center Internal Fluid Mechanics Facility," NASA TM 105187, Sept. 1991.

REPORT DOCUMENTATION PAGE

Form Approved
OMB No. 0704-0188

1. AGENCY USE ONLY (*Leave blank*)	2. REPORT DATE	3. REPORT TYPE AND DATES COVERED
	February 1993	Technical Memorandum

4. TITLE AND SUBTITLE
An Experimental Investigation of S-Duct Flow Control Using Arrays of Low-Profile Vortex Generators

5. FUNDING NUMBERS
WU-505-62-52

6. AUTHOR(S)
Bruce A. Reichert and Bruce J. Wendt

7. PERFORMING ORGANIZATION NAME(S) AND ADDRESS(ES)
National Aeronautics and Space Administration
Lewis Research Center
Cleveland, Ohio 44135-3191

8. PERFORMING ORGANIZATION REPORT NUMBER
E-7595

9. SPONSORING/MONITORING AGENCY NAMES(S) AND ADDRESS(ES)
National Aeronautics and Space Administration
Washington, D.C. 20546-0001

10. SPONSORING/MONITORING AGENCY REPORT NUMBER
NASA TM-106030

11. SUPPLEMENTARY NOTES
Prepared for the 31st Aerospace Sciences Meeting and Exhibit sponsored by the American Institute of Aeronautics and Astronautics, Reno, Nevada, January 11-14, 1993. Bruce A. Reichert, NASA Lewis Research Center and Bruce J. Wendt, National Research Council-NASA Research Associate at Lewis Research Center. Responsible person, Bruce A. Reichert, (216) 433-8397.

12a. DISTRIBUTION/AVAILABILITY STATEMENT
Unclassified - Unlimited
Subject Category 02

12b. DISTRIBUTION CODE

13. ABSTRACT (*Maximum 200 words*)

An experimental investigation was undertaken to measure the effect of various configurations of low-profile vortex generator arrays on the flow in a diffusing S-duct. Three parameters that characterize the vortex generator array were systematically varied to determine their effect: (1) the vortex generator height, (2) the streamwise location of the vortex generator array, and (3) the vortex generator spacing. Detailed measurements of total pressure at the duct exit, surface static pressure, and surface flow visualization were gathered for each vortex generator configuration. These results are reported here along with total pressure recovery and distortion coefficients determined from the experimental data. Each array of vortex generators tested improved total pressure recovery. The configuration employing the largest vortex generators was the most effective in reducing total pressure distortion but did not produce the greatest total pressure recovery. No configuration of vortex generators completely eliminated the flow separation that naturally occurs in the S-duct, however the extent of the separated flow region was reduced.

14. SUBJECT TERMS
Vortex generators, Inlet flow, Pressure recovery, Flow distortion

15. NUMBER OF PAGES
14

16. PRICE CODE
A03

17. SECURITY CLASSIFICATION OF REPORT	18. SECURITY CLASSIFICATION OF THIS PAGE	19. SECURITY CLASSIFICATION OF ABSTRACT	20. LIMITATION OF ABSTRACT
Unclassified	Unclassified	Unclassified	